Competition between d-wave superconductivity and magnetism in uniaxially strained Sr_2RuO_4

Jonas B. Hauck,[1, 2] Sophie Beck,[2] Dante M. Kennes,[1, 3] Antoine Georges,[4, 2, 5, 6] and Olivier Gingras[2]

[1]*Institute for Theoretical Solid State Physics, RWTH Aachen University and*
JARA Fundamentals of Future Information Technology, 52062 Aachen, Germany
[2]*Center for Computational Quantum Physics, Flatiron Institute,*
162 Fifth Avenue, New York, New York 10010, USA
[3]*Max Planck Institute for the Structure and Dynamics of Matter and Center Free-Electron Laser Science, Hamburg, Germany*
[4]*Collège de France, Université PSL, 11 place Marcelin Berthelot, 75005 Paris, France*
[5]*Centre de Physique Théorique, Ecole Polytechnique, CNRS,*
Institut Polytechnique de Paris, 91128 Palaiseau Cedex, France
[6]*DQMP, Université de Genève, 24 quai Ernest Ansermet, CH-1211 Genève, Suisse*
(Dated: July 20, 2023)

The pairing symmetry of Sr_2RuO_4 is a long-standing fundamental question in the physics of superconducting materials with strong electronic correlations. We use the functional renormalization group to investigate the behavior of superconductivity under uniaxial strain in a two-dimensional realistic model of Sr_2RuO_4 obtained with density functional theory and incorporating the effect of spin-orbit coupling. We find a dominant $d_{x^2-y^2}$ superconductor mostly hosted by the d_{xy}-orbital, with no other closely competing superconducting state. Within this framework we reproduce the experimentally observed enhancement of the critical temperature under strain and propose a simple mechanism driven by the density of states to explain our findings. We also investigate the competition between superconductivity and spin-density wave ordering as a function of interaction strength. By comparing theory and experiment, we discuss constraints on a possible degenerate partner of the $d_{x^2-y^2}$ superconducting state.

INTRODUCTION

Almost 30 years after the discovery of superconductivity in Sr_2RuO_4 (SRO) [1], the symmetry of its superconducting order parameter (SCOP) remains an open question. Initially, its similarities with ^{3}Helium made it a prime candidate for spin-triplet pairing [2], corroborated by various measurements [3–11]. Along with observations of time-reversal symmetry breaking (TRSB) supporting a two-component order parameter [12, 13], the superconducting (SC) state was believed for a long time to be a chiral p-wave spin-triplet. However, conflicting evidence presented in various studies remained to be explained [14, 15]. First, the presence of nodal excitations is unexpected in a chiral p-wave SC [16–19]. Second, the low critical field H_{c2} exhibited by SRO is typical for Pauli-limited spin-singlet SC [20] and the transition into the normal state upon applying a magnetic field appears to be first-order [21, 22], with indications of a Fulde-Ferrell-Larkin-Ovchinnikov state for a certain parameter range, strongly pointing to a singlet SCOP [23]. Third, no topologically protected edge states predicted in chiral p-wave states [24] were observed in experiments [25–27].

In recent years, the chiral p-wave picture has basically been dismissed. First, the careful replications of key nuclear magnetic resonance experiments previously interpreted as supporting spin-triplet pairing have highlighted a heating effect and instead concluded that the SCOP corresponds to spin-singlet pairs [28–30]. Second, applying uniaxial strain along the x principal crystallographic axis was found to enhance the critical temperature (T_c) [31, 32]. This enhancement was shown to

be maximal where the FS undergoes a Lifshitz transition, corresponding to a van Hove singularity (vHs) in the density of states (DOS), at a time-reversal invariant momentum point, inconsistent with odd-parity SCOPs like p-wave [33]. Nowadays, a consensus appears to be crystallizing around the spin-singlet and even-parity natures of the SCOP, yet the debate is still ongoing. While ultrasounds experiments support the conclusion of a two-component order parameter [34, 35] inferred by the observation of TRSB and the splitting between T_c and the TRSB transition temperature [36, 37], there are no two-temperature signature in bulk thermodynamical experiments such as specific heat and elastocalorimetry as well as scanning SQUID microscopy [38–41]. As a result of this plethora of experimental evidence, SRO can be seen both as a critical playground for testing new theories with the goal of potentially unifying some of these contradicting observations and as a testbed to verify whether our interpretations of specific experiments are valid. Either way, it constitutes an ideal system to considerably advance our understanding of the mechanisms for unconventional superconductivity [42].

Many theoretical proposals have been put forward as potential SCOPs. Initially classified as a chiral p-wave [43–49], the recent experimental evidence motivated new proposals, including $s + id$ [50–53], $d + ig$ [53–55], a combination of even and odd-parity irreducible representations (irreps) [56], E_g $d + id$ [57, 58], inter-orbital pairing [59, 60] and $d_{x^2-y^2}$ plus odd-frequency [61, 62]. A general overview of possible ordering states in terms of their irreducible representations is given in Ref. 59, 63.

In this paper, we investigate the leading supercon-

ducting instabilities of SRO using functional renormalization group (FRG) calculations [64], applied to a realistic model of the electronic structure derived from density functional theory (DFT) [65] that includes spin-orbit coupling (SOC). Note that previous studies of SRO using FRG were performed on tight-binding models, fitted to photoemission spectroscopy measurements [45, 55, 66–69]. In order to compare to experiments, we study the effect of uniaxial strain, tracking the evolution of T_c as well as the type of ordering. We find a phase diagram with two different magnetic orders that compete with a single SCOP transforming like the B_{1g} irrep (often labelled as $d_{x^2-y^2}$-wave). This competition is found to depend sensitively on the choice of interaction parameters. We show that a proper range of parameters lead to an increase of the superconducting T_c in good agreement with experiments.

RESULTS

Electronic structure. — To describe the low energy electronic structure of SRO for the different strain values, we perform *ab initio* DFT calculations downfolded onto the t_{2g} orbitals of the ruthenium atoms using maximally localized Wannier functions as detailed in the methods section. The local SOC parameter λ_{SOC} is fixed at 200 meV, consistently with the predicted correlation-induced enhancement over the DFT value and in agreement with the FS determined by photoemission experiments [70–74].

Note that the addition of SOC breaks the $SU(2)$ spin symmetry, but preserves an orbitally dependent $SU(2)$ (so called pseudospin) symmetry [62]. We keep the SOC fixed for all strain values [75].

In order to account for strong electronic correlations in this multi-orbital system, we use for most parts of this paper the $O(3)$ symmetric Hubbard-Kanamori parametrization of the interaction Hamiltonian [76], which involves two key energy scales: the on-site Hubbard repulsion U and the Hund coupling J - see methods. As done routinely in FRG calculations [43, 45, 67–69, 77–88], we neglect the flow of the self-energy in our calculations. Hence, the interaction parameters (U, J) should be considered as effective interactions with significance within our FRG framework rather than having a first-principle meaning. In this perspective, it is important to explore how the various instabilities are tuned by varying the interaction parameters.

The FS and the density of states (DOS) obtained from this downfolded t_{2g} model are displayed on Fig. 1. The left column corresponds to the unstrained system ($\epsilon_{xx} = 0$) and the right columns to the optimally uniaxially strained system for which the Fermi level is at the vHs ($\epsilon_{xx} = \epsilon_{xx}^{vHs}$). Note that ϵ_{xx}^{vHs} does not include quasiparticle renormalization and therefore is not the same value as in experiments. The D_{4h} space group symmetry of the unstrained system is lowered down to D_{2h} by
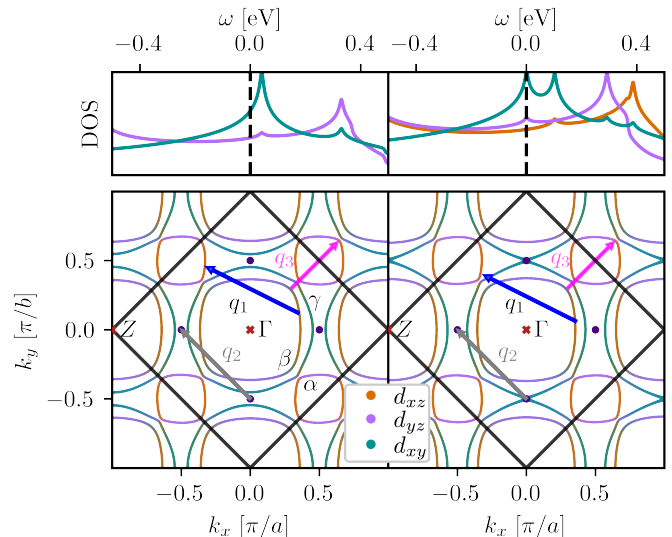

FIG. 1. Density of states (upper panels) and Fermi surface (lower panels) for the three t_{2g} orbitals of the unstrained (left) and the optimally strained (right) systems. The optimal stain of 0.8% corresponds to the system being closest to the Lifschitz transition. Here, a (b) is the lattice parameter in the x (y) direction, with $a = b$ in the $\epsilon_{xx} = 0$ case. The black dots indicates the position of the vHs of the d_{xy} orbital. The three dominant spin-density wave ordering vectors q_1, q_2 and q_3 are highlighted in black, gray and pink, respectively. The first Brillouin zone is marked by a black square. We mark the Γ and Z point by red crosses. Furthermore, we labelled the α, β and γ sheets on the FS for $\epsilon_{xx} = 0$.

uniaxial strain and the B_{1g} irreducible representation of D_{4h}, of greatest relevance to our study, turns into the A_{1g} irreducible representation of D_{2h}.

Note the slightly unusual presentation of the FS in Fig. 1: this is due to the transformation from a tetragonal basis into a x-y plane which has to be done in this fashion to ensure periodicity of the downfolded model in the two-dimensional primitive cell. Due to this, we have not a single but two k_z values in the first primitive cell, i.e. the Z-point is located at the corner of the black square.

The lowering of the symmetry under uniaxial strain lifts the degeneracy between the d_{xz} and the d_{yz} orbitals, as seen in the DOS in Fig. 1. It also splits the d_{xy} van-Hove singularity into two parts: one drifting away from the FS (x-direction) and one drifting towards the FS and crosses it at the Lifschitz transition ($\epsilon_{xx}^{vHs} \sim 0.8\%$ strain). On the FS shown in Fig. 1, we also highlight the dominant nesting vectors of the bare particle-hole susceptibility (χ_{PH}^0), see App. A. First, $q_1 = (2\pi/3a, \pi/3b)$ (and all those related by symmetry) connects the α and β sheets of the FS. Second, $q_2 = (\pi/2a, \pi/2b)$ is connecting two van-Hove singularities and should become relevant at large interactions. Third, $q_3 = (\pi/3a, \pi/3a)$ also connects the α and β sheet of the FS. These vectors are consistent with the dominant spin fluctuations observed in neutron scattering experiments [89, 90]. Note that there is a family of nesting vectors connecting α and β
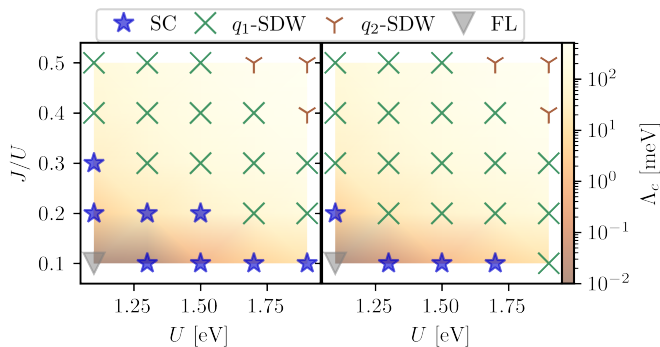
FIG. 2. Phase diagrams in the U-J parameter space for the unstrained (left) and the optimally strained (right) systems. The background color indicates the critical scale Λ_c, proportional to the ordering energy scale, with the corresponding color bar on the right. The phases are either a B_{1g} superconductor (A_{1g} under uniaxial strain), two different spin-density waves (SDWs) or a Fermi-liquid (FL). The q-vectors associated to the SDWs are shown in Fig. 1.

sheet, all close to q_1.

With these insights from the non-interacting FS and DOS in mind, we proceed with the phase diagrams as a function of U and J for the unstrained and the $\epsilon_{xx} = \epsilon_{xx}^{\text{vHs}}$ cases. The results are presented on Fig. 2. The background color corresponds to the energy scale Λ_c (expressed in meV) at which a divergence of the corresponding coupling is observed. The fastest divergent coupling corresponds to the dominant instability, which can either be superconductivity (in which case Λ_c is expected to be proportional to the Berezinskii–Kosterlitz–Thouless [91–93] critical temperature T_{BKT}) or a spin-density wave (SDW) (in which case Λ_c can be interpreted as the characteristic scale associated with the growth of the correlation length) [94]

At the lowest U and J values, we find no divergence down to the lowest energy scale resolvable with our momentum resolution, and thus conclude that the system remains in the Fermi liquid (FL) state down to that scale. Apart from this unique point, we find three types of instabilities. Up to moderate U and low but finite J, we find a $d_{x^2-y^2}$ superconducting instability (corresponding to B_{1g} symmetry for the unstrained system, turning into A_{1g} for the strained one). Upon increasing U or J, we find that the dominant instability becomes a SDW with ordering vector q_1. At even larger U and J, the system undergoes a high-temperature transition to another SDW phase characterized by the ordering vector q_2. These ordering vectors are visible in both non-interacting and interacting susceptibilities. Since we do not incorporate the effect of the self-energy, we cannot observe the shift of the q_3 peak observed in Ref. [52].

Phase diagram and magnetic orderings. — The q_1-SDW is driven by strong nesting between the α and β sheets. A corresponding peak in the spin-spin susceptibility has been well discussed both in the context of experimental observations [6, 95] and theoretical discus-

sions [61, 96]. It should be noted that this vector is connecting two different values of k_z when backfolded in the three dimensional Brillouin zone. Its in plane analog, $q_3 = (\pi/3a, \pi/3b)$, was found to be subleading in earlier three-dimensional studies using the random phase approximation (RPA) [97]. The q_3 peak is also found in DMFT calculations including vertex corrections [52, 98]. Here, we find the q_1 ordering to be the leading one, with the q_3 ordering also diverging but with smaller absolute magnitude. The increase of Λ_c can be understood in terms of the Stoner criterion being fulfilled at a larger scale for larger U or J. At higher energy scales, the vHs are strongly smeared. This effect increases the importance of the q_2 ordering vector connecting two vHs points, leading to the emergence of the q_2-SDW phase.

When applying uniaxial strain, the parameter range where we find a SDW is increased. This can be understood from the increase of the DOS at the Fermi level, which leads to a larger χ_{PH}^0 and thereby a smaller interaction is required to fulfill the Stoner criterion. Beyond this effect, straining does not affect the structures of the phases and the q_2-phase is still observable in the same parameter region, as the changes of the FS due to strain have counteracting effects: while in the y-direction the FS touches the vHs, it drifts further away from it in the x-direction.

Note that as we increase the strain beyond the Lifschitz transition, we do not find the SDW that is observed in experiments [36, 39]. The emergence of this phase has been understood as the removal of all curvature of the γ sheet between the upper/lower vHs and the X/X' points, which leads to strong nesting along this direction [99]. We do not observe this phase at any investigated strain value, possibly indicating that quasi-particle renormalization enhances the tendency towards such an instability. Further studies are required to identify the crucial ingredients for the high-strain magnetic phase.

Superconductivity. — In the following, the superconducting phase is analyzed using a linearized gap equation on the FS. As shown in Fig. 3, we find a gap that transforms according to a B_{1g} for $\epsilon_{xx} = 0$ (A_{1g} for $\epsilon_{xx} = \epsilon_{xx}^{\text{vHs}}$) representation of the D_{4h} (D_{2h}) point groups. In the band basis, this state has a dominant overlap with the $d_{x^2-y^2}$ harmonic and its main weight stems from the d_{xy} orbital. Such a type of superconductor has been observed in several other studies [50, 54, 55, 61, 62, 96, 99–101].

The spectrum of the pair-pair susceptibility at Λ_c contains the information of all possible subleading SCOPs. By analyzing this spectral distribution, we find a clear separation of the eigenvalue of the $d_{x^2-y^2}$ superconducting state by at least one order of magnitude from all eigenvalues of other SCOPs, for all parameters investigated. While this excludes any immediate degenerate state, no statement about the proximity of different symmetry states or individual critical temperatures can be drawn from FRG, because within this method the dominant instability is signalled by a divergent coupling and susceptibility. However, from the hierarchy standpoint,
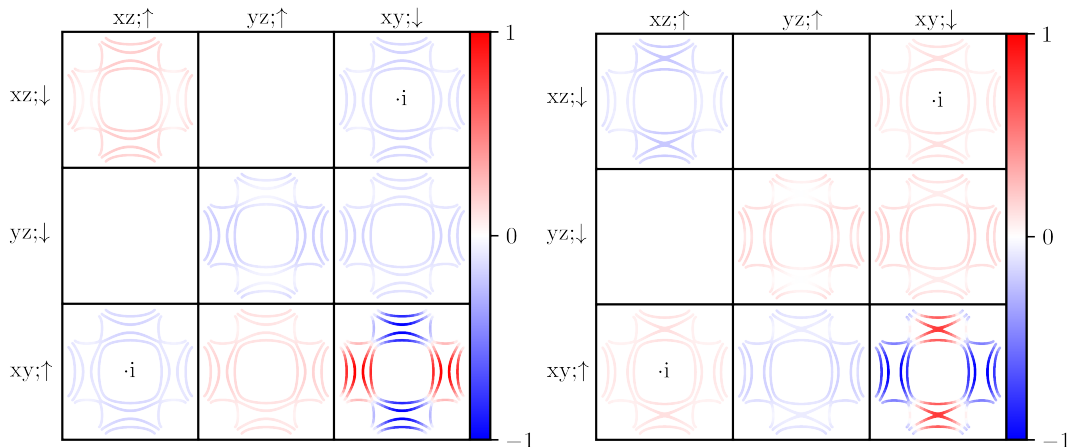
FIG. 3. Spin, orbital and momentum structure of the SCOP of Fig. 2 at $U = 1.1$ eV and $J = 0.22\,U$. Unstrained $\epsilon_{xx} = 0$ (Optimally strained $\epsilon_{xx}^{\mathrm{vHs}}$) case on the left (right). Each panel shows the momentum structure of the superconducting gap of a specific orbital pair. Since the gap function is only known up to a prefactor, we rescale it from -1 to 1, the sign and value is encoded in the colorbar. Note that only the pseudospin off-diagonal terms are non-zero, thus we only need to represent a 3×3 matrix. The SCOP transforms like the B_{1g} (A_{1g}) irreducible representation of the D_{4h} (D_{2h}) group.

we still can extract tendencies towards different orderings as discussed in App. D. This hierarchy reveals that the p-wave pairing state [43, 45, 69] is always clearly subleading by a large margin.

The superconducting phase is generated by a spin-fluctuation mechanism. The couplings U and J are crucial tuning knobs determining the onset of the phase and also control the transition to the neighbouring magnetic phase. When increasing U, the transition to a SDW is understood from the underlying ladder-type diagrams diverging as soon as U becomes larger than the critical value. Below that critical U, the still strong spin-fluctuations can drive a superconducting instability. However, increasing J has a more complex effect since it affects two different physical processes, which we discuss in terms of two distinct couplings, J_{ss} and J_{dd} in Eq. (1). J_{ss} promotes spin-flip and pair-hopping processes, thus reducing the tendency to order magnetically while also increasing pair-correlations. J_{dd} decreases inter-orbital density-density interactions, which reduces the inter-orbital repulsion between electrons on the same site. We unravel which of the two effects is most relevant for a) superconductivity and b) the magnetic transition. This is achieved by varying the two quantities independently, first in a simple RPA calculation and then in a full FRG calculation.

For the simple RPA calculation, we calculate χ_{PH}^0 at $\Lambda = 11.6$ meV. We chose $U = 0.3$ eV to circumvent the Stoner instability and vary J_{ss} and J_{dd} between $0.0U$ and $0.3U$ independently. The dominant components of the bare susceptibility are presented in Fig. 6 of App. C. In general, we observe that varying J_{ss} has barely any effect on $\chi_{\mathrm{PH}}^{\mathrm{RPA}}$. J_{dd}, on the other hand, increases the inter-orbital components by a significant amount. Therefore we expect J_{ss} to have a weaker impact on the superconducting transition. Physically this is expected since J_{ss}

hampers the spin-fluctuations which are required to obtain an effective attraction required by the superconducting state. To support this claim and understand better the underlying interference mechanism, we developed a simple 2-band toy model in App. C.

In the full FRG simulation, we verify these conclusions, i.e. increasing J_{ss} leads to a transition only at much larger values than the one for J_{dd}. See Fig. 7 of App. C. Interestingly, J_{ss} will generate a stronger admixture of higher order angular momentum superconductivity hosted by the d_{yz} and d_{xz} orbitals. These are however still sub-leading to the $d_{x^2-y^2}$ superconducting state.

Influence of strain. — Finally, we compare our results with experiments. We do so by examining the effect of strain from $\epsilon_{xx} = 0.0\%$ to $\epsilon_{xx} = 1.3\%$ on the leading instability of different (U, J) combinations. The general behavior of T_c is consistent with earlier studies [67, 99], while the predicted phases partially differ. The different critical scales Λ_c can be interpreted as an estimate for T_c of the instability. The results for all superconducting data points are summarized in Fig. 4.

For systems that start with a large initial critical scale at zero strain ($\Lambda_c(\epsilon_{xx} = 0)$), no significant enhancement with respect to strain is found. The enhancement of T_c is much larger when $\Lambda(\epsilon_{xx} = 0)$ is smaller. This effect can be understood by looking at the DOS: large energy scales, or large temperatures, correspond to smeared out features in the DOS. Thus, the shift of the vHs due to strain is irrelevant since the vHs is not resolved, i.e. the DOS at the Fermi level does not change under strain. The lower Λ_c, the sharper the vHs will become. Therefore, its shift enhances the DOS at the FS more strongly which in turn leads to a larger increase of T_c. Thus, a lower $\Lambda_c(\epsilon_{xx} = 0)$ yields an enhancement of T_c with ϵ_{xx} which is both larger and taking place over a narrower range of strain. Once the vHs has crossed the Fermi level, T_c is ex-
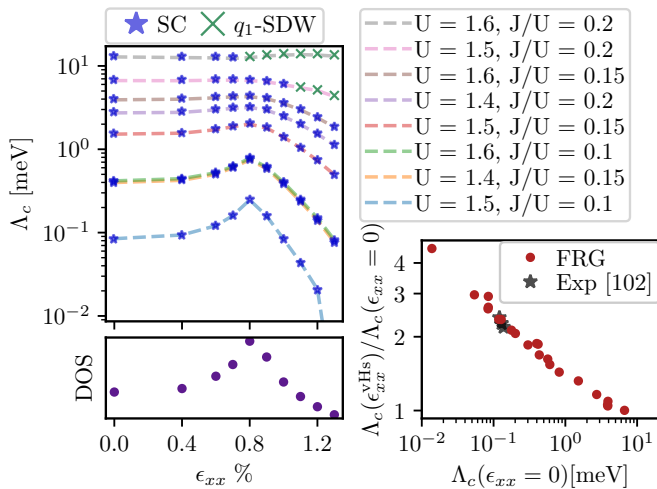
FIG. 4. Effect of strain ϵ_{xx} on the critical scale Λ_c for different values of U and J (upper left) and values of U and J for each line given in the upper right. DOS in the d_{xy} orbital depending on ϵ (lower left) and theoretically predicted enhancement of Λ_c due to uniaxial strain as a function of its value for $\epsilon_{xx} = 0$ (lower right). Each dotted line in the upper left plot corresponds to one $U - J$ combination given in the upper right. There is a clear correlation between $\Lambda_c(\epsilon_{xx} = 0)$ and the ratio of increase in T_c which can be seen in both the upper left and lower right panels. The experimental data points in the lower right plot are extracted from [102]. A proposed mechanism that explains this enhancement is detailed in the text.

pected to go down again since we rapidly reduce the DOS at the Fermi level when straining further. This proposed explanation leads to a natural experimental prediction: by studying samples of different purity, one should find different widths and heights of the enhancement.

To compare our results to experiments, we evaluate $\Lambda_c(\epsilon_{xx}^{vHs})/\Lambda_c(\epsilon_{xx} = 0)$ and plot it versus $\Lambda_c(\epsilon_{xx} = 0)$, hence measuring the increase of the critical scale depending on the initial one. We extract the corresponding experimental values from Ref. 102 by calculating the ratio of the maximal T_c and the T_c at $\epsilon_{xx} = 0$. These results are summarized in Fig. 4. We observe that the experiments indeed fit to the data predicted by FRG and we can extract a line of U and J combinations along which the experiment is reproduced. We find that the values on the line are around $U = 1.1$, 1.4 eV and $J = 0.143\,U$, $0.1\,U$. Again, we emphasize that these should be considered as effective values valid within our FRG formalism.

DISCUSSION

In summary, we studied SRO starting from a first-principles description of its electronic structure and using a diagrammatically unbiased FRG approach. Using this framework, we investigated the influence of uniaxial strain as well as different contributions of Hund's coupling. We identified that the inter-orbital interac-

tion reduction due to the density-density term J_{dd} is the main driving force favoring superconducting order, which we found to be a pseudospin-singlet $d_{x^2-y^2}$. Lastly, we showed that the experimental increase of T_c as a function of strain can be recovered on a quantitative level from FRG simulations and from a comparison to these experiments we extracted effective values of the interaction parameters.

Our results highlight the dominance of a single $d_{x^2-y^2}$ SCOP that transforms like the B_{1g} representation (A_{1g} under uniaxial strain). We note that, while this SCOP agrees with many experimental measurements, it cannot explain the evidence for two-components and time-reversal symmetry breaking. From the experimentally observed behavior of the time-reversal symmetry condition, we can infer that a partner of our found SCOP is required to remain invariant under moving the vHs through the Fermi level. This condition would be for example fulfilled by states with nodal lines along the x direction or odd-frequency superconductors [62].

An interesting direction for future studies would be to investigate the effect of interaction terms consistent with D_{4h} symmetry but breaking full cubic symmetry. This could potentially influence the competition between different low energy orders [71]. There are also many potential routes towards a more accurate investigation of the superconducting state. First, even though SRO is nearly perfectly layered, including the third spatial dimension increases the number of allowed ordering types [63]. Secondly, including frequency dependencies would allow to gauge the relevance of the proposed odd-frequency state and, importantly, allow us to begin the FRG flow from a correlated starting point i.e. from dressed quasi-particles. This offers an promising way to increase the accuracy of FRG by starting for example from a DMFT [103] description of the normal state.

METHODS

Density functional Theory. — We use density functional theory [104–106] and the Quantum ESPRESSO DFT package [107, 108] with the PBE exchange-correlation functional [109] to calculate the electronic structure. Cell parameters and internal coordinates of the crystal structure in the $I4/mmm$ space group are relaxed in the conventional cell until all force components are smaller than 1 mRy/a_0 (a_0: Bohr radius) and all components of the stress tensor are smaller than 0.5 kbar, yielding a relaxed in-plane (out-of-plane) lattice constant of $a_0 = 3.878$ Å ($c = 12.900$ Å). To calculate the strained structures, we fix one in-plane lattice constant of the conventional cell to the strained value, $a_{new} = (1 - s)a_0$, and relax the two orthogonal cell parameters as well as the internal coordinates as described above. After relaxation, we use the corresponding primitive unit cells containing one ruthenium atom each, i.e. three t_{2g} orbitals. We use scalar-relativistic ultrasoft pseudopoten-

tials from the GBRV library [110], with the $4s$ and $4p$ ($2s$) semicore states for both strontium and ruthenium (for oxygen) atoms included in the valence. The energy cutoffs for the wave functions and charge density are set to 60 Ry and 720 Ry, respectively. We use a $12 \times 12 \times 12$ Monkhorst–Pack k-point grid to sample the Brillouin zone, and a smearing of 0.01 Ry utilizing the Methfessel–Paxton scheme. To describe the low-energy physics we construct three ruthenium-centered t_{2g}-like maximally localized Wannier functions for each strained structure using Wannier90 [111–113]. Spin-orbit coupling is included by first performing the DFT calculation without it and then adding a local SOC $\lambda_{\mathrm{SOC}} = 200$ meV to account for the correlation-induced enhancement over the DFT value.

Functional renormalization group. — In order to account for strong local electronic correlations in this multi-orbital system, we consider the Hubbard-Kanamori interaction Hamiltonian [76]

$$
\begin{aligned}
\hat{H}_{\mathrm{int}} = & \sum_{il} U \hat{n}_{il}^{\uparrow} \hat{n}_{il}^{\downarrow} + \sum_{il_1 \neq l_2} (U - 2J_{dd}) \hat{n}_{il_1}^{\uparrow} \hat{n}_{il_2}^{\downarrow} \\
& + \sum_{i\sigma l_1 \neq l_2} (U - 3J_{dd}) \hat{n}_{il_1}^{\sigma} \hat{n}_{il_2}^{\sigma} \\
& - \sum_{il_1 \neq l_2} J_{ss} \hat{c}_{il_1}^{\uparrow,\dagger} \hat{c}_{il_1}^{\downarrow} \hat{c}_{il_2}^{\downarrow,\dagger} \hat{c}_{il_2}^{\uparrow} + \sum_{il_1 \neq l_2} J_{ss} \hat{c}_{il_1}^{\uparrow,\dagger} \hat{c}_{il_1}^{\downarrow,\dagger} \hat{c}_{il_2}^{\downarrow} \hat{c}_{il_2}^{\uparrow}
\end{aligned} \tag{1}
$$

where U is the intra-orbital on-site Coulomb repulsion, while J_{dd} (J_{ss}) is the density-density (spin-flip and pair hoping) part of the Hund's coupling. In the rotationally invariant formulation where $O(3)$ symmetry is satisfied, $J_{dd} = J_{ss}$.

The strong electronic correlations emerging from the Hubbard-Kanamori interactions are incorporated to the non-interacting downfolded systems using the functional renormalization group (FRG) [64, 114]. FRG is technically an exact method to calculate the effective action functional of a given quantum action. It does so by introducing a scale-dependent cutoff (here we use a sharp energy cutoff) in the non-interacting propagator of the system. By taking derivatives with respect to this cutoff, one generates an infinite hierarchy of flow equations. In practice, this hierarchy must be truncated to become numerically tractable, making the method pertubatively motivated.

In this work, we employ the standard level-2 truncation, neglecting all three and more particle vertices. The validity of this approximation in the weak-to-intermediate coupling regime can be motivated by a power-counting argument to prove the RG-irrelevance of higher order terms [64]. Furthermore, we neglect the frequency dependence of the interaction, again motivated

by the power counting argument, and the self-energy. This approach was applied to various systems including SRO [43, 45, 67–69, 77–88] and can be viewed as an diagrammatically unbiased extension of the random phase approximation.

In practice, we solve the flow equations from an energy scale much larger than the bandwidth and then integrate towards lower energies until we hit a divergence in one of the three diagrammatic channels labelled the particle-particle (PP), particle-hole (PH) and crossed particle-hole ($\overline{\mathrm{PH}}$) channels. A divergence is associated to a phase transition as the corresponding susceptibility also diverges. Information of the ordering type can be extracted from the susceptibilities as well as linearized gap equations [115].

We employ the truncated unity approximation which allows us to reduce the memory required computationally [116–118].

For the FRG simulations, we use the TU^{2}FRG code [118]. For convergence, we include all form-factors up to a distance of 8.2 Å, which amounts to a total number of 75 basis functions per orbital in the unit cell. We checked for convergence by increasing the number of form-factors included near the phase transition between the magnetic and the superconducting phase for a few data points in the phase diagram. The simulations are performed on a 36×36 momentum-mesh in the $x - y$ plane for the vertex function. The loop integration is performed using a FFT approach and an additional refinement of 45×45 is employed to achieve higher energy resolution. The results of the integration do not differ upon changing the resolution of the loop integration.

By using an enhanced value of the SOC, the effects of local interactions on SOC are already included on the single-particle level of the calculations. We do not suffer from double counting at that level since we neglect the flow of the self-energy. As a consequence however, our calculation does not take into account the renormalized effective mass of quasi-particles.

[1] Y. Maeno, H. Hashimoto, K. Yoshida, S. Nishizaki, T. Fujita, J. G. Bednorz, and F. Lichtenberg, Superconductivity in a layered perovskite without copper, Nature

372, 532 (1994).

[2] T. Rice and M. Sigrist, Sr_2RuO_4: an electronic analogue of ^{3}He?, Journal of Physics: Condensed Matter **7**, L643 (1995).

[3] K. Ishida, H. Mukuda, Y. Kitaoka, K. Asayama, Z. Mao, Y. Mori, and Y. Maeno, Spin-triplet superconductivity in Sr_2RuO_4 identified by ^{17}O knight shift, Nature **396**, 658 (1998).

[4] K. Ishida, M. Manago, T. Yamanaka, H. Fukazawa, Z. Q. Mao, Y. Maeno, and K. Miyake, Spin polarization enhanced by spin-triplet pairing in Sr_2RuO_4 probed by NMR, Phys. Rev. B **92**, 100502 (2015).

[5] J. A. Duffy, S. M. Hayden, Y. Maeno, Z. Mao, J. Kulda, and G. J. McIntyre, Polarized-neutron scattering study of the cooper-pair moment in Sr_2RuO_4, Phys. Rev. Lett. **85**, 5412 (2000).

[6] M. Braden, Y. Sidis, P. Bourges, P. Pfeuty, J. Kulda, Z. Mao, and Y. Maeno, Inelastic neutron scattering study of magnetic excitations in Sr_2RuO_4, Phys. Rev. B **66**, 064522 (2002).

[7] Y. Liu, K. Nelson, Z. Mao, R. Jin, and Y. Maeno, Tunneling and phase-sensitive studies of the pairing symmetry in Sr_2RuO_4, Journal of low temperature physics **131**, 1059 (2003).

[8] K. Nelson, Z. Mao, Y. Maeno, and Y. Liu, Odd-parity superconductivity in Sr_2RuO_4, Science **306**, 1151 (2004).

[9] Y. Liu, Phase-sensitive-measurement determination of odd-parity, spin-triplet superconductivity in Sr_2RuO_4, New Journal of Physics **12**, 075001 (2010).

[10] K. Deguchi, Z. Q. Mao, H. Yaguchi, and Y. Maeno, Gap structure of the spin-triplet superconductor Sr_2RuO_4 determined from the field-orientation dependence of the specific heat, Phys. Rev. Lett. **92**, 047002 (2004).

[11] C. Lupien, W. A. MacFarlane, C. Proust, L. Taillefer, Z. Q. Mao, and Y. Maeno, Ultrasound attenuation in Sr_2RuO_4: An angle-resolved study of the superconducting gap function, Phys. Rev. Lett. **86**, 5986 (2001).

[12] J. Xia, Y. Maeno, P. T. Beyersdorf, M. M. Fejer, and A. Kapitulnik, High resolution polar kerr effect measurements of Sr_2RuO_4: Evidence for broken time-reversal symmetry in the superconducting state, Phys. Rev. Lett. **97**, 167002 (2006).

[13] G. M. Luke, Y. Fudamoto, K. Kojima, M. Larkin, J. Merrin, B. Nachumi, Y. Uemura, Y. Maeno, Z. Mao, Y. Mori, *et al.*, Time-reversal symmetry-breaking superconductivity in Sr_2RuO_4, Nature **394**, 558 (1998).

[14] A. P. Mackenzie and Y. Maeno, The superconductivity of Sr_2RuO_4 and the physics of spin-triplet pairing, Rev. Mod. Phys. **75**, 657 (2003).

[15] Y. Maeno, S. Kittaka, T. Nomura, S. Yonezawa, and K. Ishida, Evaluation of spin-triplet superconductivity in Sr_2RuO_4, Journal of the Physical Society of Japan **81**, 011009 (2012), https://doi.org/10.1143/JPSJ.81.011009.

[16] K. Izawa, H. Takahashi, H. Yamaguchi, Y. Matsuda, M. Suzuki, T. Sasaki, T. Fukase, Y. Yoshida, R. Settai, and Y. Onuki, Superconducting gap structure of spin-triplet superconductor Sr_2RuO_4 studied by thermal conductivity, Phys. Rev. Lett. **86**, 2653 (2001).

[17] E. Hassinger, P. Bourgeois-Hope, H. Taniguchi, S. René de Cotret, G. Grissonnanche, M. S. Anwar, Y. Maeno, N. Doiron-Leyraud, and L. Taillefer, Vertical line nodes in the superconducting gap structure of Sr_2RuO_4, Phys. Rev. X **7**, 011032 (2017).

[18] M. A. Tanatar, M. Suzuki, S. Nagai, Z. Q. Mao, Y. Maeno, and T. Ishiguro, Anisotropy of magnetothermal conductivity in Sr_2RuO_4, Phys. Rev. Lett. **86**, 2649 (2001).

[19] S. NishiZaki, Y. Maeno, and Z. Mao, Changes in the superconducting state of Sr_2RuO_4 under magnetic fields probed by specific heat, Journal of the Physical Society of Japan **69**, 572 (2000), https://doi.org/10.1143/JPSJ.69.572.

[20] F. Jerzembeck, A. Steppke, A. Pustogow, Y. Luo, A. Chronister, D. A. Sokolov, N. Kikugawa, Y.-S. Li, M. Nicklas, S. E. Brown, A. P. Mackenzie, and C. W. Hicks, Upper critical field of Sr_2RuO_4 under in-plane uniaxial pressure, Phys. Rev. B **107**, 064509 (2023).

[21] S. Kittaka, A. Kasahara, T. Sakakibara, D. Shibata, S. Yonezawa, Y. Maeno, K. Tenya, and K. Machida, Sharp magnetization jump at the first-order superconducting transition in Sr_2RuO_4, Phys. Rev. B **90**, 220502 (2014).

[22] S. Yonezawa, T. Kajikawa, and Y. Maeno, Specific-heat evidence of the first-order superconducting transition in Sr_2RuO_4, Journal of the Physical Society of Japan **83**, 083706 (2014), https://doi.org/10.7566/JPSJ.83.083706.

[23] K. Kinjo, M. Manago, S. Kitagawa, Z. Mao, S. Yonezawa, Y. Maeno, and K. Ishida, Superconducting spin smecticity evidencing the fulde-ferrell-larkin-ovchinnikov state in Sr_2RuO_4, Science **376**, 397 (2022).

[24] T. Scaffidi and S. H. Simon, Large chern number and edge currents in Sr_2RuO_4, Phys. Rev. Lett. **115**, 087003 (2015).

[25] J. R. Kirtley, C. Kallin, C. W. Hicks, E.-A. Kim, Y. Liu, K. A. Moler, Y. Maeno, and K. D. Nelson, Upper limit on spontaneous supercurrents in Sr_2RuO_4, Phys. Rev. B **76**, 014526 (2007).

[26] C. W. Hicks, J. R. Kirtley, T. M. Lippman, N. C. Koshnick, M. E. Huber, Y. Maeno, W. M. Yuhasz, M. B. Maple, and K. A. Moler, Limits on superconductivity-related magnetization in sr_2ruo_4 and $pros_4sb_{12}$ from scanning squid microscopy, Phys. Rev. B **81**, 214501 (2010).

[27] P. J. Curran, S. J. Bending, W. M. Desoky, A. S. Gibbs, S. L. Lee, and A. P. Mackenzie, Search for spontaneous edge currents and vortex imaging in Sr_2RuO_4 mesostructures, Phys. Rev. B **89**, 144504 (2014).

[28] A. Pustogow, Y. Luo, A. Chronister, Y.-S. Su, D. Sokolov, F. Jerzembeck, A. P. Mackenzie, C. W. Hicks, N. Kikugawa, S. Raghu, *et al.*, Constraints on the superconducting order parameter in Sr_2RuO_4 from oxygen-17 nuclear magnetic resonance, Nature **574**, 72 (2019).

[29] K. Ishida, M. Manago, K. Kinjo, and Y. Maeno, Reduction of the ^{17}O knight shift in the superconducting state and the heat-up effect by NMR pulses on Sr_2RuO_4, Journal of the Physical Society of Japan **89**, 034712 (2020).

[30] A. N. Petsch, M. Zhu, M. Enderle, Z. Q. Mao, Y. Maeno, I. I. Mazin, and S. M. Hayden, Reduction of the spin susceptibility in the superconducting state of Sr_2RuO_4 observed by polarized neutron scattering, Phys. Rev. Lett. **125**, 217004 (2020).

[31] C. A. Watson, A. S. Gibbs, A. P. Mackenzie, C. W. Hicks, and K. A. Moler, Micron-scale measurements of

low anisotropic strain response of local T_c in Sr_2RuO_4, Phys. Rev. B **98**, 094521 (2018).

[32] A. Steppke, L. Zhao, M. E. Barber, T. Scaffidi, F. Jerzembeck, H. Rosner, A. S. Gibbs, Y. Maeno, S. H. Simon, A. P. Mackenzie, *et al.*, Strong peak in T_c of Sr_2RuO_4 under uniaxial pressure, Science **355**, eaaf9398 (2017).

[33] V. Sunko, E. Abarca Morales, I. Marković, M. E. Barber, D. Milosavljević, F. Mazzola, D. A. Sokolov, N. Kikugawa, C. Cacho, P. Dudin, H. Rosner, C. W. Hicks, P. D. C. King, and A. P. Mackenzie, Direct observation of a uniaxial stress-driven Lifshitz transition in Sr_2RuO_4, npj Quantum Materials **4**, 46 (2019).

[34] S. Benhabib, C. Lupien, I. Paul, L. Berges, M. Dion, M. Nardone, A. Zitouni, Z. Q. Mao, Y. Maeno, A. Georges, L. Taillefer, and C. Proust, Ultrasound evidence for a two-component superconducting order parameter in sr2ruo4, Nature Physics **17**, 194 (2021).

[35] S. Ghosh, A. Shekhter, F. Jerzembeck, N. Kikugawa, D. A. Sokolov, M. Brando, A. P. Mackenzie, C. W. Hicks, and B. J. Ramshaw, Thermodynamic evidence for a two-component superconducting order parameter in sr2ruo4, Nature Physics **17**, 199 (2021).

[36] V. Grinenko, S. Ghosh, R. Sarkar, J.-C. Orain, A. Nikitin, M. Elender, D. Das, Z. Guguchia, F. Brückner, M. E. Barber, J. Park, N. Kikugawa, D. A. Sokolov, J. S. Bobowski, T. Miyoshi, Y. Maeno, A. P. Mackenzie, H. Luetkens, C. W. Hicks, and H.-H. Klauss, Split superconducting and time-reversal symmetry-breaking transitions in Sr_2RuO_4 under stress, Nature Physics **17**, 748 (2021).

[37] V. Grinenko, R. Sarkar, S. Ghosh, D. Das, Z. Guguchia, H. Luetkens, I. Shipulin, A. Ramires, N. Kikugawa, Y. Maeno, K. Ishida, C. W. Hicks, and H.-H. Klauss, μSR measurements on Sr_2RuO_4 under $\langle 110 \rangle$ uniaxial stress, Phys. Rev. B **107**, 024508 (2023).

[38] Y.-S. Li, N. Kikugawa, D. A. Sokolov, F. Jerzembeck, A. S. Gibbs, Y. Maeno, C. W. Hicks, J. Schmalian, M. Nicklas, and A. P. Mackenzie, High-sensitivity heat-capacity measurements on Sr_2RuO_4 under uniaxial pressure, Proceedings of the National Academy of Sciences **118**, e2020492118 (2021), https://www.pnas.org/doi/pdf/10.1073/pnas.2020492118.

[39] Y.-S. Li, M. Garst, J. Schmalian, S. Ghosh, N. Kikugawa, D. A. Sokolov, C. W. Hicks, F. Jerzembeck, M. S. Ikeda, Z. Hu, *et al.*, Elastocaloric determination of the phase diagram of Sr_2RuO_4, Nature **607**, 276 (2022).

[40] G. Palle, C. Hicks, R. Valentí, Z. Hu, Y.-S. Li, A. Rost, M. Nicklas, A. P. Mackenzie, and J. Schmalian, Constraints on the superconducting state of Sr_2RuO_4 from elastocaloric measurements (2023), arXiv:2304.07182 [cond-mat.supr-con].

[41] E. Mueller, Y. Iguchi, C. Watson, C. Hicks, Y. Maeno, and K. Moler, Constraints on a split superconducting transition under uniaxial strain in sr2ruo4 from scanning squid microscopy (2023), arXiv:2306.13737 [cond-mat.supr-con].

[42] A. P. Mackenzie, T. Scaffidi, C. W. Hicks, and Y. Maeno, Even odder after twenty-three years: the superconducting order parameter puzzle of Sr_2RuO_4, npj Quantum Materials **2**, 40 (2017).

[43] Q. H. Wang, C. Platt, Y. Yang, C. Honerkamp, F. C. Zhang, W. Hanke, T. M. Rice, and R. Thomale, Theory of superconductivity in a three-orbital model of Sr_2RuO_4, Europhysics Letters **104**, 17013 (2013).

[44] M. Tsuchiizu, Y. Yamakawa, S. Onari, Y. Ohno, and H. Kontani, Spin-triplet superconductivity in Sr_2RuO_4 due to orbital and spin fluctuations: Analyses by two-dimensional renormalization group theory and self-consistent vertex-correction method, Phys. Rev. B **91**, 155103 (2015).

[45] W.-S. Wang, C.-C. Zhang, F.-C. Zhang, and Q.-H. Wang, Theory of chiral p-wave superconductivity with near nodes for Sr_2RuO_4, Phys. Rev. Lett. **122**, 027002 (2019).

[46] L.-D. Zhang, W. Huang, F. Yang, and H. Yao, Superconducting pairing in Sr_2RuO_4 from weak to intermediate coupling, Phys. Rev. B **97**, 060510 (2018).

[47] T. Scaffidi, J. C. Romers, and S. H. Simon, Pairing symmetry and dominant band in Sr_2RuO_4, Phys. Rev. B **89**, 220510 (2014).

[48] A. Ramires and M. Sigrist, Identifying detrimental effects for multiorbital superconductivity: Application to Sr_2RuO_4, Phys. Rev. B **94**, 104501 (2016).

[49] S. Acharya, D. Pashov, C. Weber, H. Park, L. Sponza, and M. V. Schilfgaarde, Evening out the spin and charge parity to increase t_c in Sr_2RuO_4, Communications Physics **2**, 163 (2019).

[50] A. T. Rømer, P. J. Hirschfeld, and B. M. Andersen, Superconducting state of Sr_2RuO_4 in the presence of longer-range coulomb interactions, Phys. Rev. B **104**, 064507 (2021).

[51] A. T. Rømer, T. A. Maier, A. Kreisel, P. J. Hirschfeld, and B. M. Andersen, Leading superconducting instabilities in three-dimensional models for Sr_2RuO_4, Phys. Rev. Res. **4**, 033011 (2022).

[52] C.-Y. Moon, Effects of orbital selective dynamical correlation on the spin susceptibility and superconducting symmetries in Sr_2RuO_4 (2023), arXiv:2303.13910 [cond-mat.str-el].

[53] H. S. Røising, G. Wagner, M. Roig, A. T. Rømer, and B. M. Andersen, Heat capacity double transitions in time-reversal symmetry broken superconductors, Phys. Rev. B **106**, 174518 (2022).

[54] Y. Sheng, Y. Li, and Y.-f. Yang, Multipole-fluctuation pairing mechanism of $d_{x^2-y^2} + ig$ superconductivity in Sr_2RuO_4, Phys. Rev. B **106**, 054516 (2022).

[55] X. Wang, Z. Wang, and C. Kallin, Higher angular momentum pairing states in Sr_2RuO_4 in the presence of longer-range interactions, Phys. Rev. B **106**, 134512 (2022).

[56] T. Scaffidi, Degeneracy between even- and odd-parity superconductivity in the quasi-one-dimensional hubbard model and implications for Sr_2RuO_4, Phys. Rev. B **107**, 014505 (2023).

[57] H. G. Suh, H. Menke, P. M. R. Brydon, C. Timm, A. Ramires, and D. F. Agterberg, Stabilizing even-parity chiral superconductivity in Sr_2RuO_4, Physical Review Research **2**, 032023 (2020).

[58] S. Beck, A. Hampel, M. Zingl, C. Timm, and A. Ramires, Effects of strain in multiorbital superconductors: The case of Sr_2RuO_4, Phys. Rev. Res. **4**, 023060 (2022).

[59] S.-O. Kaba and D. Sénéchal, Group-theoretical classification of superconducting states of strontium ruthenate, Physical Review B **100**, 10.1103/physrevb.100.214507 (2019).

[60] S. Ando, S. Ikegaya, S. Tamura, Y. Tanaka, and K. Yada, Surface state of the interorbital pairing state in the sr$_2$ruo$_4$ superconductor, Phys. Rev. B **106**, 214520 (2022).

[61] O. Gingras, R. Nourafkan, A.-M. S. Tremblay, and M. Côté, Superconducting Symmetries of Sr$_2$RuO$_4$ from First-Principles Electronic Structure, Physical Review Letters **123**, 217005 (2019).

[62] O. Gingras, N. Allaglo, R. Nourafkan, M. Côté, and A.-M. S. Tremblay, Superconductivity in correlated multiorbital systems with spin-orbit coupling: Coexistence of even- and odd-frequency pairing, and the case of Sr$_2$RuO$_4$, Physical Review B **106**, 064513 (2022).

[63] A. Ramires and M. Sigrist, Superconducting order parameter of Sr$_2$RuO$_4$: A microscopic perspective, Phys. Rev. B **100**, 104501 (2019).

[64] W. Metzner, M. Salmhofer, C. Honerkamp, V. Meden, and K. Schönhammer, Functional renormalization group approach to correlated fermion systems, Reviews of Modern Physics **84**, 299 (2012), arXiv: 1105.5289.

[65] W. Kohn and L. J. Sham, Self-consistent equations including exchange and correlation effects, Phys. Rev. **140**, A1133 (1965).

[66] Q. Wang, C. Platt, Y. Yang, C. Honerkamp, F. Zhang, W. Hanke, T. Rice, and R. Thomale, Theory of superconductivity in a three-orbital model of Sr$_2$RuO$_4$, EPL (Europhysics Letters) **104**, 17013 (2013).

[67] Y.-C. Liu, F.-C. Zhang, T. M. Rice, and Q.-H. Wang, Theory of the evolution of superconductivity in Sr$_2$RuO$_4$ under anisotropic strain, npj Quantum Materials **2**, 10.1038/s41535-017-0014-y (2017).

[68] Z. Wang, X. Wang, and C. Kallin, Spin-orbit coupling and spin-triplet pairing symmetry in Sr$_2$RuO$_4$, Phys. Rev. B **101**, 064507 (2020).

[69] Y.-C. Liu, W.-S. Wang, F.-C. Zhang, and Q.-H. Wang, Superconductivity in Sr$_2$RuO$_4$ thin films under biaxial strain, Phys. Rev. B **97**, 224522 (2018).

[70] E. Pavarini and I. I. Mazin, First-principles study of spin-orbit effects and NMR in Sr$_2$RuO$_4$, Phys. Rev. B **74**, 035115 (2006).

[71] G. Zhang, E. Gorelov, E. Sarvestani, and E. Pavarini, Fermi surface of Sr$_2$RuO$_4$: Spin-orbit and anisotropic coulomb interaction effects, Phys. Rev. Lett. **116**, 106402 (2016).

[72] M. Kim, J. Mravlje, M. Ferrero, O. Parcollet, and A. Georges, Spin-orbit coupling and electronic correlations in sr$_2$ruo$_4$, Phys. Rev. Lett. **120**, 126401 (2018).

[73] A. Damascelli, D. H. Lu, K. M. Shen, N. P. Armitage, F. Ronning, D. L. Feng, C. Kim, Z.-X. Shen, T. Kimura, Y. Tokura, Z. Q. Mao, and Y. Maeno, Fermi surface, surface states, and surface reconstruction in Sr$_2$RuO$_4$, Phys. Rev. Lett. **85**, 5194 (2000).

[74] A. Tamai, M. Zingl, E. Rozbicki, E. Cappelli, S. Riccò, A. de la Torre, S. McKeown Walker, F. Bruno, P. King, W. Meevasana, M. Shi, M. Radović, N. Plumb, A. Gibbs, A. Mackenzie, C. Berthod, H. Strand, M. Kim, A. Georges, and F. Baumberger, High-Resolution Photoemission on Sr$_2$RuO$_4$ Reveals Correlation-Enhanced Effective Spin-Orbit Coupling and Dominantly Local Self-Energies, Physical Review X **9**, 021048 (2019).

[75] Unpublished DMFT data shows that the corrections of the SOC due to strain are negligible.

[76] J. Kanamori, Electron correlation and ferromagnetism of transition metals, Progress of Theoretical Physics **30**, 275 (1963).

[77] M. M. Scherer, D. M. Kennes, and L. Classen, Chiral superconductivity with enhanced quantized hall responses in moiré transition metal dichalcogenides, npj Quantum Materials **7**, 100 (2022).

[78] L. Klebl, A. Fischer, L. Classen, M. M. Scherer, and D. M. Kennes, Competition of density waves and superconductivity in twisted tungsten diselenide, Physical Review Research **5**, 10.1103/physrevresearch.5.l012034 (2023).

[79] N. Gneist, L. Classen, and M. M. Scherer, Competing instabilities of the extended hubbard model on the triangular lattice: Truncated-unity functional renormalization group and application to moiré materials, Phys. Rev. B **106**, 125141 (2022).

[80] M. L. Kiesel, C. Platt, W. Hanke, and R. Thomale, Model evidence of an anisotropic chiral $d+id$-wave pairing state for the water-intercalated Na$_x$CoO$_2$·yH$_2$O superconductor, Phys. Rev. Lett. **111**, 097001 (2013).

[81] M. L. Kiesel, C. Platt, and R. Thomale, Unconventional fermi surface instabilities in the kagome hubbard model, Phys. Rev. Lett. **110**, 126405 (2013).

[82] J. Beyer, J. B. Hauck, L. Klebl, T. Schwemmer, D. M. Kennes, R. Thomale, C. Honerkamp, and S. Rachel, Rashba spin-orbit coupling in the square-lattice hubbard model: A truncated-unity functional renormalization group study, Phys. Rev. B **107**, 125115 (2023).

[83] M. L. Kiesel, C. Platt, W. Hanke, D. A. Abanin, and R. Thomale, Competing many-body instabilities and unconventional superconductivity in graphene, Phys. Rev. B **86**, 020507 (2012).

[84] J. B. Hauck, C. Honerkamp, S. Achilles, and D. M. Kennes, Electronic instabilities in penrose quasicrystals: Competition, coexistence, and collaboration of order, Physical Review Research **3**, 10.1103/physrevresearch.3.023180 (2021).

[85] J. Ehrlich and C. Honerkamp, Functional renormalization group for fermion lattice models in three dimensions: Application to the hubbard model on the cubic lattice, Phys. Rev. B **102**, 195108 (2020).

[86] L. Klebl, D. M. Kennes, and C. Honerkamp, Functional renormalization group for a large moiré unit cell, Phys. Rev. B **102**, 085109 (2020).

[87] D. S. de la Peña, J. Lichtenstein, C. Honerkamp, and M. M. Scherer, Antiferromagnetism and competing charge instabilities of electrons in strained graphene from coulomb interactions, Phys. Rev. B **96**, 205155 (2017).

[88] S.-J. O, Y.-H. Kim, H.-Y. Rim, H.-C. Pak, and S.-J. Im, Effect of exchange interaction on electronic instabilities in the honeycomb lattice: A functional renormalization group study, Phys. Rev. B **99**, 245140 (2019).

[89] K. Iida, M. Kofu, N. Katayama, J. Lee, R. Kajimoto, Y. Inamura, M. Nakamura, M. Arai, Y. Yoshida, M. Fujita, K. Yamada, and S.-H. Lee, Inelastic neutron scattering study of the magnetic fluctuations in sr$_2$ruo$_4$, Phys. Rev. B **84**, 060402 (2011).

[90] P. Steffens, Y. Sidis, J. Kulda, Z. Q. Mao, Y. Maeno, I. I. Mazin, and M. Braden, Spin fluctuations in Sr$_2$RuO$_4$ from polarized neutron scattering: Implications for superconductivity, Phys. Rev. Lett. **122**, 047004 (2019).

[91] V. Berezinskii, Destruction of long-range order in one-dimensional and two-dimensional systems having a continuous symmetry group i. classical systems, Sov. Phys. JETP **32**, 493 (1971).

[92] V. Berezinskii, Destruction of long-range order in one-dimensional and two-dimensional systems possessing a continuous symmetry group. ii. quantum systems, Sov. Phys. JETP **34**, 610 (1972).

[93] J. M. Kosterlitz and D. J. Thouless, Ordering, metastability and phase transitions in two-dimensional systems, Journal of Physics C: Solid State Physics **6**, 1181 (1973).

[94] Because of Mermin-Wagner theorem (which is not obeyed by FRG), a finite T_c is expected for the BKT transition into the SC phase, while $T_c = 0$ for an SDW breaking $SU(2)$.

[95] K. Iida, J. Lee, M. B. Stone, M. Kofu, Y. Yoshida, and S. Lee, Two-dimensional incommensurate magnetic fluctuations in sr2(ru0.99ti0.01)o4, Journal of the Physical Society of Japan **81**, 124710 (2012), https://doi.org/10.1143/JPSJ.81.124710.

[96] A. T. Rømer, T. A. Maier, A. Kreisel, P. J. Hirschfeld, and B. M. Andersen, Leading superconducting instabilities in three-dimensional models for Sr_2RuO_4, Physical Review Research **4**, 033011 (2022).

[97] A. T. Rømer, T. A. Maier, A. Kreisel, P. Hirschfeld, and B. M. Andersen, Leading superconducting instabilities in three-dimensional models for Sr_2RuO_4, Physical Review Research **4**, 033011 (2022).

[98] H. U. R. Strand, M. Zingl, N. Wentzell, O. Parcollet, and A. Georges, Physical Review B **100**, 10.1103/physrevb.100.125120 (2019).

[99] A. T. Rømer, A. Kreisel, M. A. Müller, P. J. Hirschfeld, I. M. Eremin, and B. M. Andersen, Theory of strain-induced magnetic order and splitting of T_c and $T_{\rm trsb}$ in Sr_2RuO_4, Phys. Rev. B **102**, 054506 (2020).

[100] A. T. Rømer, P. J. Hirschfeld, and B. M. Andersen, Superconducting state of Sr_2RuO_4 in the presence of longer-range Coulomb interactions, PHYSICAL REVIEW B , 16 (2021).

[101] M. Roig, A. T. Rømer, A. Kreisel, P. J. Hirschfeld, and B. M. Andersen, Superconductivity in multiorbital systems with repulsive interactions: Hund's pairing versus spin-fluctuation pairing, Phys. Rev. B **106**, L100501 (2022).

[102] A. Steppke, L. Zhao, M. E. Barber, T. Scaffidi, F. Jerzembeck, H. Rosner, A. S. Gibbs, Y. Maeno, S. H. Simon, A. P. Mackenzie, and C. W. Hicks, Strong peak in Tc of Sr_2RuO_4 under uniaxial pressure, Science **355**, eaaf9398 (2017), publisher: American Association for the Advancement of Science.

[103] C. Taranto, S. Andergassen, J. Bauer, K. Held, A. Katanin, W. Metzner, G. Rohringer, and A. Toschi, From infinite to two dimensions through the functional renormalization group, Phys. Rev. Lett. **112**, 196402 (2014).

[104] W. Kohn and L. J. Sham, Self-Consistent Equations Including Exchange and Correlation Effects, Physical Review **140**, A1133 (1965).

[105] P. Hohenberg and W. Kohn, Inhomogeneous Electron Gas, Physical Review **136**, B864 (1964), publisher: American Physical Society.

[106] W. Kohn, A. D. Becke, and R. G. Parr, Density Functional Theory of Electronic Structure, The Journal of Physical Chemistry **100**, 12974 (1996).

[107] P. Giannozzi, S. Baroni, N. Bonini, M. Calandra, R. Car, C. Cavazzoni, D. Ceresoli, G. L. Chiarotti, M. Cococcioni, I. Dabo, *et al.*, Quantum espresso: a modular and open-source software project for quantum simulations of materials, Journal of physics: Condensed matter **21**, 395502 (2009).

[108] P. Giannozzi, O. Andreussi, T. Brumme, O. Bunau, M. B. Nardelli, M. Calandra, R. Car, C. Cavazzoni, D. Ceresoli, M. Cococcioni, N. Colonna, I. Carnimeo, A. D. Corso, S. de Gironcoli, P. Delugas, R. A. DiStasio, A. Ferretti, A. Floris, G. Fratesi, G. Fugallo, R. Gebauer, U. Gerstmann, F. Giustino, T. Gorni, J. Jia, M. Kawamura, H.-Y. Ko, A. Kokalj, E. Küç ükbenli, M. Lazzeri, M. Marsili, N. Marzari, F. Mauri, N. L. Nguyen, H.-V. Nguyen, A. O. de-la Roza, L. Paulatto, S. Poncé, D. Rocca, R. Sabatini, B. Santra, M. Schlipf, A. P. Seitsonen, A. Smogunov, I. Timrov, T. Thonhauser, P. Umari, N. Vast, X. Wu, and S. Baroni, Advanced capabilities for materials modelling with quantum ESPRESSO, Journal of Physics: Condensed Matter **29**, 465901 (2017).

[109] J. P. Perdew, K. Burke, and M. Ernzerhof, Generalized gradient approximation made simple, Phys. Rev. Lett. **77**, 3865 (1996).

[110] K. F. Garrity, J. W. Bennett, K. M. Rabe, and D. Vanderbilt, Pseudopotentials for high-throughput dft calculations, Computational Materials Science **81**, 446 (2014).

[111] A. A. Mostofi, J. R. Yates, Y.-S. Lee, I. Souza, D. Vanderbilt, and N. Marzari, wannier90: A tool for obtaining maximally-localised wannier functions, Computer Physics Communications **178**, 685 (2008).

[112] A. A. Mostofi, J. R. Yates, G. Pizzi, Y.-S. Lee, I. Souza, D. Vanderbilt, and N. Marzari, An updated version of wannier90: A tool for obtaining maximally-localised wannier functions, Computer Physics Communications **185**, 2309 (2014).

[113] G. Pizzi, V. Vitale, R. Arita, S. Blügel, F. Freimuth, G. Géranton, M. Gibertini, D. Gresch, C. Johnson, T. Koretsune, J. Ibañez-Azpiroz, H. Lee, J.-M. Lihm, D. Marchand, A. Marrazzo, Y. Mokrousov, J. I. Mustafa, Y. Nohara, Y. Nomura, L. Paulatto, S. Poncé, T. Ponweiser, J. Qiao, F. Thöle, S. S. Tsirkin, M. Wierzbowska, N. Marzari, D. Vanderbilt, I. Souza, A. A. Mostofi, and J. R. Yates, Wannier90 as a community code: new features and applications, Journal of Physics: Condensed Matter **32**, 165902 (2020).

[114] N. Dupuis, L. Canet, A. Eichhorn, W. Metzner, J. Pawlowski, M. Tissier, and N. Wschebor, The nonperturbative functional renormalization group and its applications, Physics Reports **910**, 1 (2021), the nonperturbative functional renormalization group and its applications.

[115] J. Beyer, J. B. Hauck, and L. Klebl, Reference results for the momentum space functional renormalization group, The European Physical Journal B **95**, 10.1140/epjb/s10051-022-00323-y (2022).

[116] C. Husemann and M. Salmhofer, Efficient parametrization of the vertex function, Ω scheme, and the t, t' hubbard model at van hove filling, Phys. Rev. B **79**, 195125 (2009).

[117] J. Lichtenstein, D. S. de la Peña, D. Rohe, E. D. Napoli, C. Honerkamp, and S. Maier, High-performance functional renormalization group calculations for interacting

fermions, Computer Physics Communications **213**, 100 (2017).

[118] J. B. Hauck and D. M. Kennes, TU^{2}FRG: a scalable approach for truncated unity functional renormalization group in generic fermionic models, The European Physical Journal B **95**, 10.1140/epjb/s10051-022-00316-x (2022).

[119] Jülich Supercomputing Centre, JURECA: Data Centric and Booster Modules implementing the Modular Supercomputing Architecture at Jülich Supercomputing Centre, Journal of large-scale research facilities **7**, 10.17815/jlsrf-7-182 (2021).

[120] N. E. Bickers, Self-Consistent Many-Body Theory for Condensed Matter Systems, in *Theoretical Methods for Strongly Correlated Electrons*, CRM Series in Mathematical Physics, edited by D. Sénéchal, A.-M. Tremblay, and C. Bourbonnais (Springer, 2004) pp. 237–296.

Appendix A: Particle-hole susceptibility

In the main text, we explained how we can extract the value of effective parameters of the interaction suitable in FRG, here we found $U = 1.1$ eV and $J = 0.143\,U$. With these extracted values, we compute the interacting particle-hole susceptibility χ_{PH} at $T = 464$ K, shown on a two-dimensional momentum-grid in Fig. 5. We compare with χ_{PH} obtained by solving the Bethe-Salpeter equation with a vertex extracted using DMFT [98]. FRG clearly overestimates the correlations at the X-point and on the connection line between X and M, similarly to what is obtained using the random phase approximation [61, 62]. Beyond that, FRG reproduces roughly the same shape and structure of the susceptibility as DMFT,
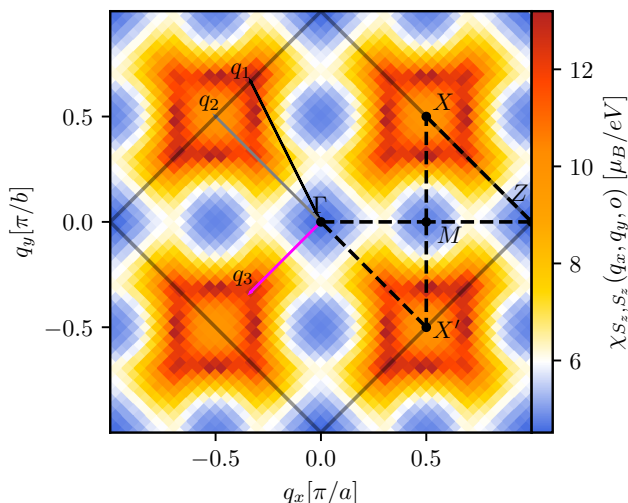

FIG. 5. Interacting particle-hole susceptibility at $\Lambda = 464$ K obtained with FRG at the extracted experimental interaction parameters $U = 1.1$ eV and $J = 0.143\,U$. The color scale is adapted to the one of Ref. [98]. We again mark the first BZ as a black square and draw the $k_z = 0$ irreducible path as dotted lines.

but cannot reproduce its shifting of the peaks [52, 98]. As discussed in App. D, correcting for this overestimation in the effective interaction might influence the critical energy scales, but is not expected to drastically alter the hierarchy of the different order parameters. Most critically, we show analytically that the leading SDW peak observed in experiments [90] will also lead to an attractive interaction in the singlet channel.

Appendix B: Even- vs odd-parity pairing

Here we show the numerical ratio between the leading even-parity (the B_{1g} d-wave reported in the main text) and the leading odd-parity eigenvalues for different points in $U - J$ space near the boundary with the q_1-SDW phase in Fig. 2. We find that the even-parity d-wave state always has a much bigger eigenvalue, signaling its dominance. Note that while there is a clear separation between these eigenvalues, this does not fully exclude a competition since the odd-parity solution could diverge at slightly lower energy scales and yet appear to have a relatively much smaller eigenvalue. This dominating behavior of the even-parity state is in contradiction with earlier SM-FRG studies [43, 45, 69]. A possible discrepancy between our work and theirs is the starting non-interacting model. Moreover, one can observe that although it remains very small, the ratio $\lambda_p/\lambda_{d_{x^2-y^2}}$ becomes slightly larger when approaching the SDW transition.

While this is a clear separation on the level of the leading eigenvalues, a clear separation in terms of the critical energy scale of the two phases is harder to be extracted, since we flow into a divergence this ratio is bound to be very small except if the critical scale of two phases are very close to each other. Thus these results only indicate that the critical energy scales are separated at least slightly and grow closer when approaching the magnetic transition without ever interchanging the order. A stronger argument can be made by looking at how many other eigenvectors are between the leading d-wave and the leading odd-parity one. We consistently find, throughout the phase diagram, at least 20 other even-parity eigenvectors between them. Thus we can safely conclude that odd-parity is far from dominant.

Appendix C: Effects of J_{dd} and J_{ss}

In the following, we analyze analytically the effects of J_{ss} and J_{dd} in a simplified $SU(2)$ symmetric two-orbital model. The non-interacting model is assumed to be given by

$$\hat{H} = \sum_l \sum_{ij} t_{ij}(c_{li}^\dagger c_{lj} + c_{lj}^\dagger c_{li}) \tag{C1}$$

where l is an orbital and i, j are sites. We first examine the magnetic channel susceptibility which is given in the
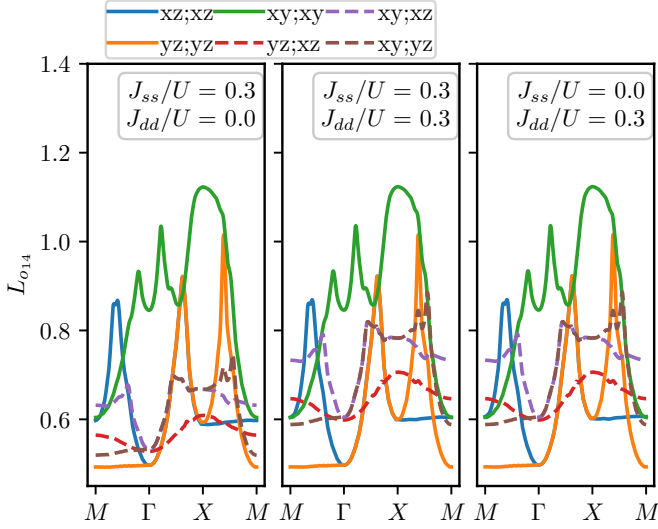
FIG. 6. Effects of J_{dd} and J_{ss} on the interacting Suszeptibility obtained from RPA at $U = 0.3$ and $\Lambda = 1$meV.
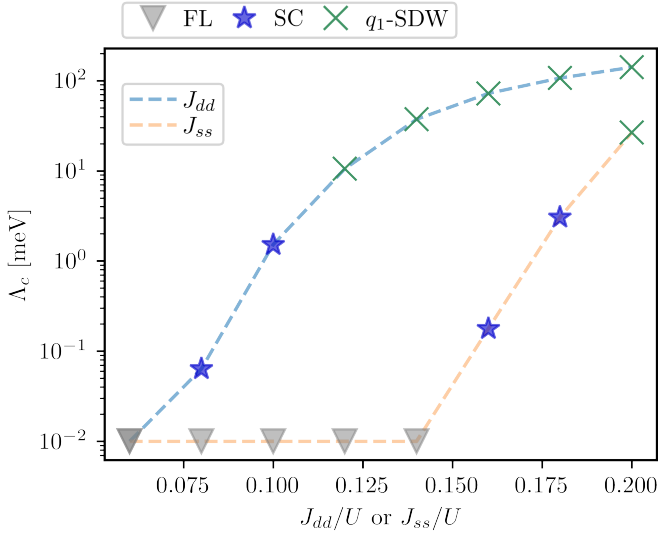

FIG. 7. Effects of J_{dd} and J_{ss} on the FRG flow results. We observe that J_{dd} drives the transition to an ordered state quicker than J_{ss} indicating that for the underlying interaction mechanism it is beneficial to have smaller inter-orbital coupling.

two-particle basis $|l_1\rangle \otimes |l_2\rangle$. The components of the bare particle-hole susceptibility are given by

$$[\chi^0_{\mathrm{PH}}(Q)]^{l_1 l_2 l_3 l_4}_{KK'} \propto G^{l_1 l_3}_{K+Q} G^{l_4 l_2}_K \delta_{KK'} \qquad (C2)$$

where G is the one-particle Green's function and K, K' and Q are four-momenta [62, 120]. From this expression, we find that the bare particle-hole susceptibility is diagonal in orbital space. Presuming the two orbitals to be degenerate, we write

$$\chi^0_{\mathrm{PH}} = \begin{pmatrix} \chi_1 & 0 & 0 & 0 \\ 0 & \chi_2 & 0 & 0 \\ 0 & 0 & \chi_2 & 0 \\ 0 & 0 & 0 & \chi_1 \end{pmatrix}. \qquad (C3)$$

In RPA, the vertex is the anti-symmetric static and local Coulomb tensor. We spin-diagonalize it and take the magnetic channel, which generates spin-fluctuations. We have

$$\Gamma = \begin{pmatrix} U & 0 & 0 & J_{ph} \\ 0 & U - 2J_{dd} & J_{sf} & 0 \\ 0 & J_{sf} & U - 2J_{dd} & 0 \\ J_{ph} & 0 & 0 & U \end{pmatrix}, \qquad (C4)$$

where the pair-hopping and spin-flip terms are characterized by J_{ph} and J_{sf} respectively. Consequently, the eigenvalues of $\Gamma \chi^0_{\mathrm{PH}}$ are

$$\lambda = \chi_1(U \pm J_{ph}), \; \chi_2(U - 2J_{dd} \pm J_{sf}) \qquad (C5)$$

with eigenvectors

$$\begin{pmatrix} 1 \\ 0 \\ 0 \\ \pm 1 \end{pmatrix} \quad \text{and} \quad \begin{pmatrix} 0 \\ 1 \\ \pm 1 \\ 0 \end{pmatrix}. \qquad (C6)$$

In other words, a pair on l_1 can constructively or destructively interfere with a pair on l_2 via J_{ph}, which enhances the intra-orbital components of the susceptibility. On the other hand, J_{sf} enhances the inter-orbital components. On the other hand, J_{dd} acts in the same way as spin flips, affecting only the inter-orbital components of the interacting susceptibility. However it has twice the magnitude. Which terms play what role also crucially depends on the signs of χ_1 and χ_2;

The corresponding numerical experiments are visualized in Fig. 6. They quantify the effects of the two different couplings and help to gauge their importance for the phase diagram.

Appendix D: Driving fluctuations analysis

Here, we want to construct a more in depth understanding of which spin-fluctuations are responsible for which pairing instabilities. To this end, we focus on the d_{xy} orbital again assuming $SU(2)$ symmetry. Therefore we restrict the analysis to the spin-singlet sector. The spin-triplet can be obtained by employing the crossing relations. Furthermore, we assume an attractive interaction obtained from RPA like spin-fluctuation $C(q)$, i.e. without fermionic momentum dependencies. The starting point for this discussion is the linearized gap equation, which can be rewritten as

$$\lambda \Delta_{o_1, o_2}(k) = \Gamma^P_{o_1, o_2; o'_3, o'_4}(q = 0, k, k')$$
$$\times \chi_{o'_3, o'_4; o_3, o_4}(k') \Delta_{o_3, o_4}(k') \qquad (D1)$$

where summation over repeated indices is implicit. We arrive to a simpler picture by transforming this equation to real-space, introducing the lattice vectors b. We write

$$\Delta_{o_1, o_2}(b) = e^{-ik \cdot b} \Delta_{o_1, o_2}(k), \qquad (D2)$$

which leads us to

$$\lambda \Delta_{o_1,o_2}(b) = \Gamma^P_{o_1,o_2;o'_3,o'_4}(b,b')$$
$$\times \chi_{o'_3,o'_4;o_3,o_4}(b',b'')\Delta_{o_3,o_4}(b''). \quad (D3)$$

Now, we are mainly interested in nearest neighbor superconductivity, thus restricting the allowed b to nearest neighbor form-factors. The two central quantities in the linearized gap equation are the particle-particle loop $\chi_{o'_3,o'_4;o_3,o_4}(b',b'')$ and the P-channel vertex $\Gamma^P_{o_1,o_2;o'_3,o'_4}(b,b')$, which in the following we construct for a specific choice of a symmetrized basis for the $d_{x^2-y^2}$ and the extended s-wave SCOPs for a purely spin-fluctuation interaction $C(q_C = k + k' - q_P)$. For this we introduce the symmetrized form-factors denoted by $f_b(k)$:

$$\Gamma^P(q_P = 0, b, b) = \frac{1}{4} \int dk\, dk'\, dr\, (\cos(k_x) \pm \cos(k_y))(\cos(k'_x) \pm \cos(k'_y))e^{ir(k+k')}C(r)$$
$$= \frac{1}{4}\left[C(r_x = 1, r_y = 0) + C(r_x = -1, r_y = 0) + C(r_x = 0, r_y = 1) + C(r_x = 0, r_y = -1)\right]. \quad (D4)$$

From this we observe immediately two things: First, a pure spin-spin interaction does not differentiate between extended s-wave or $d_{x^2-y^2}$ (or p_x and p_y). It merely gives a numerical prefactor to be put into the gap equation. Secondly, that prefactor is just dependent on the value of $C(r)$ for r on the nearest neighbors; i.e. as long as the Fourier transform of C is attractive on the nearest neighbor, we generate even superconductivity whose symmetry is determined by the particle-particle loops fermionic argument only.

$$C(r) = \int dq\, e^{iqr}C(q) \quad (D5)$$

For now, lets assume that $C(q)$ (again we focus on the d_{xy} orbital) is consisting of δ-peaks at q_2 or q_1/q_3 with unit weight. This allows us to calculate the Fourier transformation $C(r)$ analytically. We focus on $C(r_x = 1, r_y = 0)$, since all other terms can be understood via symmetries. We find $C(r_x = 1, r_y = 0; q_2) = -1$ and $C(r_x = 1, r_y = 0; q_1) = e^{i2\pi/3}$, meaning that $P(q_2) = -1$ and $P(q_1) = -0.5$. Thus the overestimation of correlations at X amplifies tendency towards superconductivity, but not towards one specific type. In more general terms, any transfer momentum of the form $q_i = (q, q)$ will generate attraction in the even channel as long as $rq_i > \pi/2$. Below this threshold, the Fourier transformation of $C(q)$ will become positive and thus generate attractive interactions in the odd-channel. Thus also the predicted leading momentum transfer found in DMFT should generate attraction for a singlet state.